

A DNA-Micropatterned Surface for Propagating Biomolecular Signals by Positional on-off Assembly of Catalytic Nanocompartments

Viviana Maffeis, Dimitri Hürlimann, Agata Krywko-Cendrowska, Cora-Ann Schoenenberger, Catherine E. Housecroft,* and Cornelia G. Palivan*

Signal transduction is pivotal for the transfer of information between and within living cells. The composition and spatial organization of specified compartments are key to propagating soluble signals. Here, a high-throughput platform mimicking multistep signal transduction which is based on a geometrically defined array of immobilized catalytic nanocompartments (CNCs) that consist of distinct polymeric nanoassemblies encapsulating enzymes and DNA or enzymes alone is presented. The dual role of single entities or tandem CNCs in providing confined but communicating spaces for complex metabolic reactions and in protecting encapsulated compounds from denaturation is explored. To support a controlled spatial organization of CNCs, CNCs are patterned by means of DNA hybridization to a microprinted glass surface. Specifically, CNC-functionalized DNA microarrays are produced where individual reaction compartments are kept in close proximity by a distinct geometrical arrangement to promote effective communication. Besides a remarkable versatility and robustness, the most prominent feature of this platform is the reversibility of DNA-mediated CNC-anchoring which renders it reusable. Micropatterns of polymer-based nanocompartment assemblies offer an ideal scaffold for the development of the next generation responsive and communicative soft-matter analytical devices for applications in catalysis and medicine.

controlled polymer network formation, and surface patterning, in general, any application that requires a specific sequence of events. A precise spatiotemporal control is equally essential for most biological processes involved in signaling and cellular communication. The quest for control over reactions has led to the development of a plethora of synthetic tools with chemoselectivity, regioselectivity, and/or stereoselectivity that allow us to build molecular frameworks with complex architectures. Nanopatterning techniques and molecular printing, defined as processes where molecules or materials are directly transferred to a substrate of interest in the form of submicrometer features with at least one dimension on the molecular scale, have remarkably enhanced the prospects of controlling the properties for applications in regenerative medicine and tissue engineering. In this regard, two technologies—soft lithography^[1,2] and dip-pen nanolithography^[3,4]—have emerged as the most widely used molecular printing

methods for forming desired features on a wide variety of substrates. Recently, DNA has been used as a bio-ink for the fabrication of robust functional materials for healthcare, drug delivery, biosensing, bioimaging, nanotechnology, and electronic applications.^[5,6] DNA-ink printed materials, in particular patterned surfaces lend themselves to the attachment of other materials that expand their functions.^[7,8] By combining different immobilization strategies to attach specific supramolecular assemblies on a surface, locally defined patterns with designated properties at high spatial organization are achieved that result in an increased functionality and complexity.^[9] Accordingly, coimmobilization of functional, nanosized assemblies, such as micelles, polymersomes, or nanoparticles broadens the possibility to engineer functionalized active surfaces with nanostructured textures for catalysis, biosensing and the development of point-of-care devices.^[10–12] Considerable efforts have been made to develop compartments in which specific enzymatic reactions take place, or that can support cascade reactions.^[13–16] Of particular interest are nanometric compartments (polymersomes), with their hollow spherical architecture, as they allow inclusion of hydrophilic molecules inside their lumen (e.g., enzymes)

1. Introduction


Controlling where and when a reaction occurs is critical for many applications including polymer synthesis/modification,

V. Maffeis, D. Hürlimann, A. Krywko-Cendrowska, C.-A. Schoenenberger, C. E. Housecroft, C. G. Palivan
Department of Chemistry
University of Basel

Mattenstrasse 24a, BPR 1096, Basel 4058, Switzerland
E-mail: catherine.housecroft@unibas.ch; cornelia.palivan@unibas.ch

V. Maffeis, D. Hürlimann, C.-A. Schoenenberger, C. E. Housecroft, C. G. Palivan

NCCR-Molecular Systems Engineering
BPR 1095, Mattenstrasse 24a, Basel CH-4058, Switzerland

 The ORCID identification number(s) for the author(s) of this article can be found under <https://doi.org/10.1002/smll.202202818>.

© 2022 The Authors. Small published by Wiley-VCH GmbH. This is an open access article under the terms of the Creative Commons Attribution-NonCommercial-NoDerivs License, which permits use and distribution in any medium, provided the original work is properly cited, the use is non-commercial and no modifications or adaptations are made.

DOI: 10.1002/smll.202202818

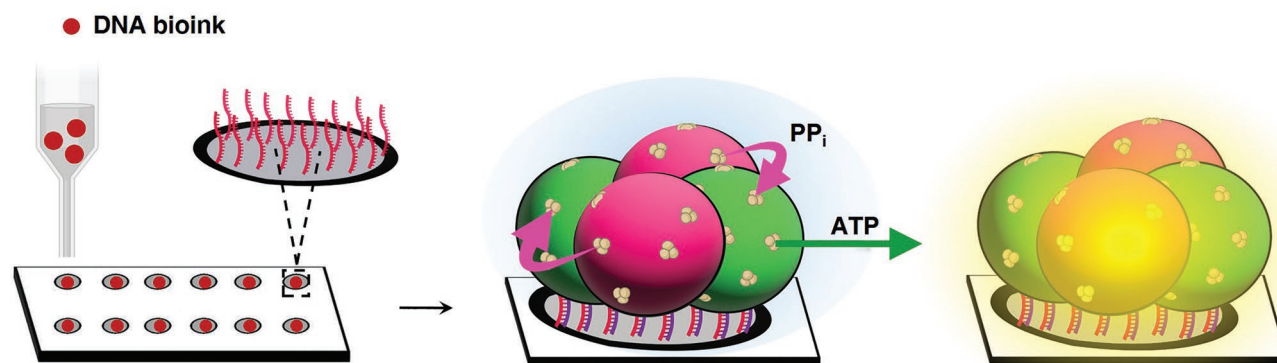


Figure 1. 3D view of micropatterned CNC immobilization promoting a cascade reaction between two distinct CNCs that ultimately results in a bioluminescent surface. The light is produced by the travelling of cascade products or signaling molecules (pink arrows) from one type of CNC to the next. The ATP generated by the downstream CNC is needed for producing bioluminescence. The signaling pathway involves diffusion through melittin pores.

and/or hydrophobic molecules such as membrane proteins, in their membrane.^[17,18] Notably, polymersomes show improved stability compared to lipid-based vesicles, and allow tuning of their properties, such as membrane thickness, polarity, or toxicity, based on the chemical versatility of the polymer building blocks.^[19] Moreover, it is possible to modify their surface with biological molecules that mediate cellular targeting or surface attachment or, as recently shown, the self-organization of polymersomes into clusters.^[20,21] The controlled distance between enzymes encapsulated in different nanocompartments working in tandem has been found to be essential in the optimization of natural and man-made cascade reactions.^[22] Adequate spacing aids in counteracting limiting factors, such as diffusion across membranes, and increases the overall efficiency of the system. Furthermore, nanocompartments are ideally suited to protect active agents (enzymes, proteins, drugs) by shielding them from harsh environments, or by controlling their location or release profile.^[17,18,23] In particular, enzymes that are often rapidly degraded in complex biological environments, which limits their efficacy to short time periods, are safeguarded inside polymersomes and their activity is prolonged.^[23] The efficiency of enzyme cascades, however, depends not only on the activity of individual enzyme but is influenced by the amplification of regulatory inputs as well as for the integration of different regulatory signals. Here we present a microarray of protein-loaded nanocompartments promoting a cascade reaction between the compartments and resulting in dual functionality: a sensing device for DNA polymerization and a transducer for biomolecular signals. For this purpose, we took advantage of complementary DNA hybridization to obtain a micropattern of communicating compartments immobilized on dots printed with DNA-ink on a glass surface (**Figure 1**). We first created two types of catalytic nanocompartments (CNCs) working in tandem: one that contained the Klenow fragment of DNA Polymerase I and a single-stranded DNA (ssDNA) template (Klenow CNC), and the other containing ATP sulfurylase (ATP sulfurylase CNC). Both CNCs were generated by self-assembly of amphiphilic poly(dimethylsiloxane)-block-poly(2-methyl-2-oxazoline) (PDMS-*b*-PMOXA) diblock copolymer in the presence of respective biomolecules and melittin,^[24] a pore forming peptide,

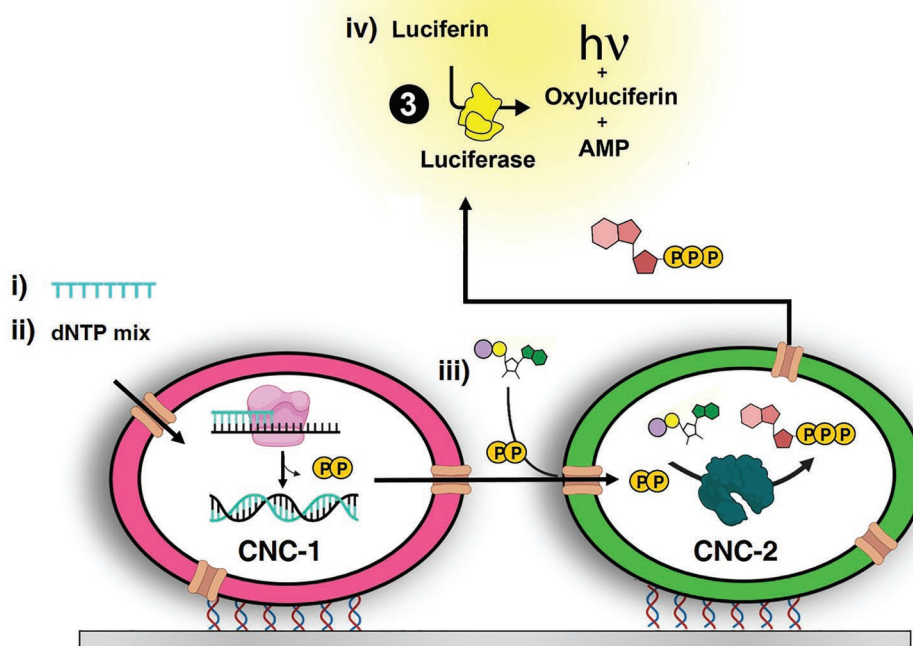
which served to permeabilize the membrane for the exchange of selected molecular cargoes. Second, we used microcontact printing of ssDNA on a glass surface to ultimately afford by DNA hybridization an architecture of nanocompartments that represents the steps of a signal transduction cascade. CNCs were immobilized on a patterned surface at specific locations to promote the communication between the different functional nanocompartments. Moreover, by using hybridization of complementary DNA strands as an immobilization strategy, we aimed to gain reusability of the DNA-microprinted surface by repeated cycles of polymersome-loading and removal. Together, the control associated with the microcontact printing of ssDNA and that involving segregated reaction spaces at the nanoscale open new avenues in a variety of applications where propagating biomolecular signals is essential.

2. Results and Discussion

2.1. DNA Polymerase and ATP Sulfurylase CNCs

The model signal transduction cascade consists of a 3-step enzymatic reaction involving Klenow fragment of DNA polymerase I,^[25] ATP sulfurylase,^[26] and firefly luciferase^[27] (**Figure 2**). In the first step, double-stranded DNA is synthesized from a single-stranded template, and inorganic pyrophosphate (PP_i), quantitatively related to the number of nucleotides incorporated, is released from CNC-1 (pink) and enters CNC-2 (green). The ATP sulfurylase inside CNC-2 then catalyzes the transfer of the PP_i to adenosine 5'-phosphosulfate, resulting in the production of ATP. At the end of the cascade, the ATP set free by CNC-2 activates the surrounding luciferase to catalyze the oxidation of luciferin to oxyluciferin and carbon dioxide along with a burst of light detectable at 560 nm. Hence, DNA synthesis is quantitatively reported by the production of light.

As a building block for the CNCs, we used PMOXA₁₀-*b*-PDMS₂₅, an amphiphilic poly(2-methyl-2-oxazoline)-*block*-poly(dimethyl-siloxane) diblock copolymer (**Figure 3**; and Figures S1 and S2, Supporting Information) which was shown to self-assemble via film rehydration into polymeric vesicles



Cascade step:

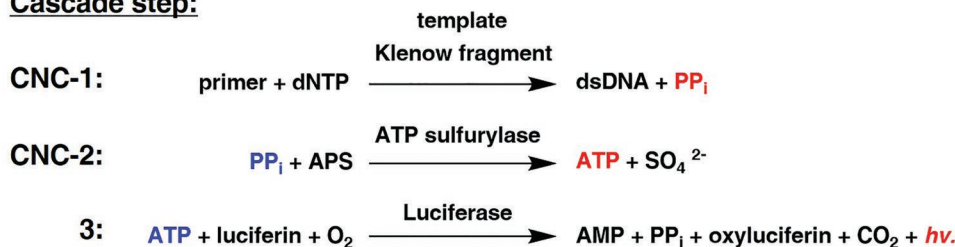


Figure 2. Slice through a sender-receiver system for biomolecular signal propagation. Scheme of the cascade reaction involving 3 different enzymes: two of which are individually encapsulated in CNCs that are immobilized on a surface and one which is free in solution. The bio-products PP_i and ATP generated by the activity of CNC-1 (pink) and CNC-2 (green), respectively, act as signals in the cascade that ultimately generates luminescence as readout for DNA synthesis.

with a membrane thickness of 12 nm ± 0.8.^[28] Copolymers with PDMS as hydrophobic block and PMOXA as hydrophilic block are well suited for producing catalytic compartments because the polymer membrane is generally impermeable to small molecules but sufficiently flexible to enable the insertion of membrane proteins^[29] and pore forming peptides such as melittin that enable communication with the compartment interior.^[30] Accordingly, in situ catalysis has been achieved by luciferase^[31] or glucuronidase^[32] confined in the hydrophilic cavity of melittin-permeabilized PMOXA₁₀-b-PDMS₂₅ based polymersomes. Melittin has been shown to induce pore formation in membranes formed by triblock PMOXA-PDMS-PMOXA and diblock PMOXA-PDMS without destabilizing the vesicles.^[29] Melittin insertion in polymeric membranes strongly depends

on the copolymer features and membrane properties such as thickness and curvature.^[29] Melittin pore formation is dynamic and the pore size reported for lipid membranes vary from 0.4^[33] to 1.7 nm.^[34] A number of substrates including glucose, AmplexRed^[29] and 4-methylumbelliferyl glucuronide^[32] and the respective products have been shown to diffuse via melittin pores in and out of polymersomes.

Self-assembly of polymersomes encapsulating either Klenow fragment of polymerase I and template DNA (Klenow CNCs) or ATP sulfurylase (ATP sulfurylase CNCs) was induced by rehydration of thin films of PMOXA₁₀-PDMS₂₅ by an aqueous solution containing melittin (Figure 3A). The resulting nanoassemblies were extruded through 200 nm pore diameter membranes to decrease the size polydispersity. The physical characterization

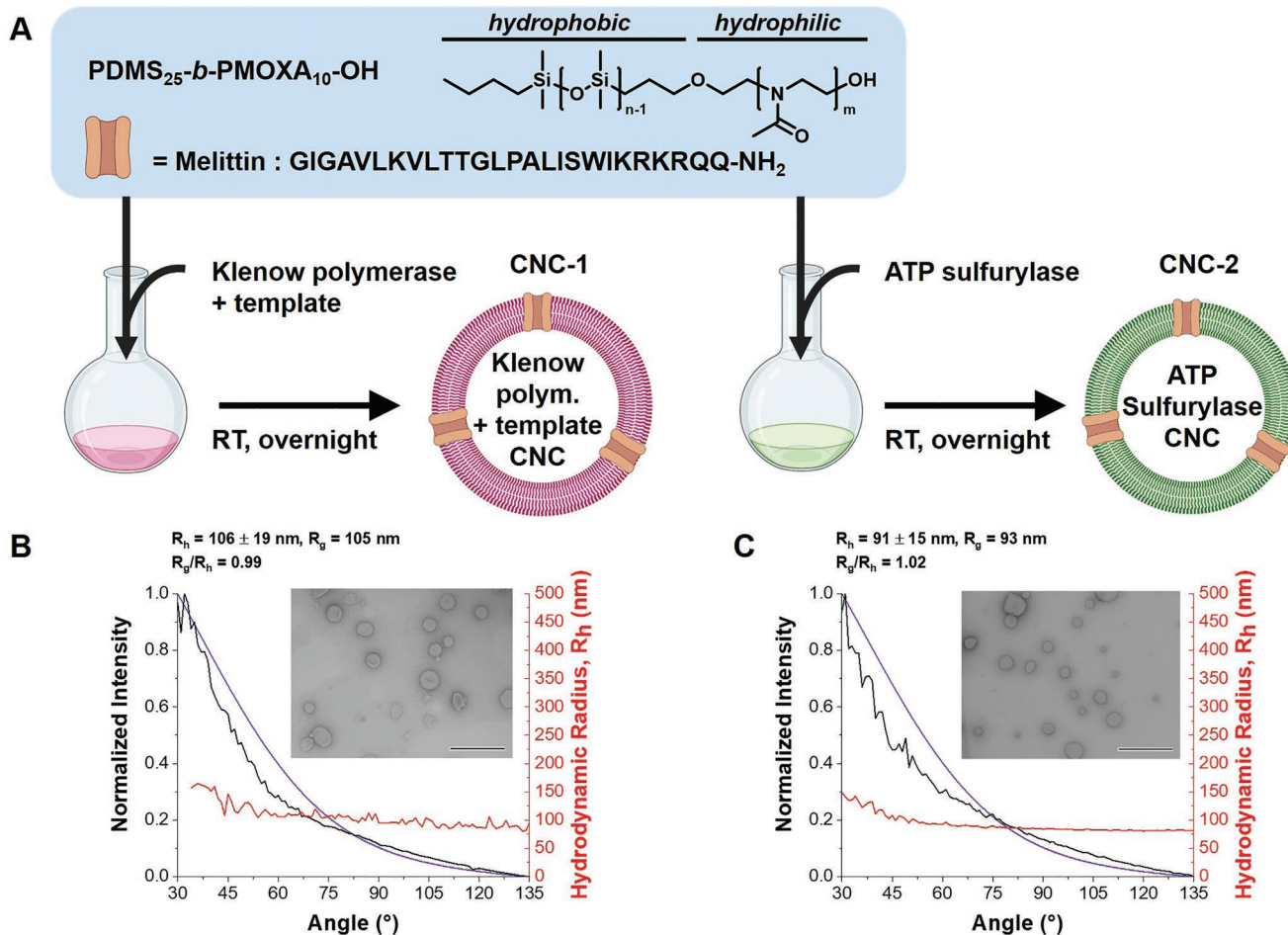


Figure 3. Design and characterization of CNC-1 and CNC-2. A) Schematic representation of the self-assembly process to generate bioinspired catalytic nanocompartments. B) Size determination by static light scattering (SLS) and dynamic light scattering (DLS) of melittin-permeabilized Klenow CNC (PDI = 0.18) with corresponding transmission electron microscopy (TEM) image (inset). Scale bar, 500 nm. C) Size determination by SLS and DLS of melittin-permeabilized ATP sulfurylase CNC (PDI = 0.16) with corresponding TEM image (inset). Scale bar, 500 nm.

of the assemblies by static light scattering (SLS) and dynamic light scattering (DLS) showed that Klenow CNCs had a hydrodynamic radius (R_h) of 106 ± 19 nm and a radius of gyration (R_g) of 105 nm (Figure 3B), whereas ATP sulfurylase-CNCs appeared slightly smaller at R_h 91 ± 15 nm and R_g 93 nm, respectively (Figure 3C). Corresponding CNCs that were not permeabilized with melittin were similar in size (Figure S3, Supporting Information). The ratio between R_h and R_g , close to 1 in both cases, is indicative of a vesicular structure of the assemblies produced. Consistently, transmission electron microscopy (TEM) micrographs revealed the deformed spherical morphology typical of polymersomes for permeabilized (Figure 3B,C) and nonpermeabilized CNCs (Figure S4, Supporting Information). The encapsulation of enzymes in polymersomes neither changed their size, nor induced aggregation. Nanoparticle tracking analysis (NTA) indicated a similar particle concentration for Klenow- and ATP sulfurylase CNCs with 3.45×10^{11} and 4.28×10^{11} particles mL^{-1} , respectively (Table S1, Supporting Information).

To further characterize Klenow CNCs, we studied the encapsulation of template DNA in CNCs by fluorescence correlation

spectroscopy (FCS) (Table S2, Supporting Information).^[35] FCS measures the fluorescence fluctuations due to the Brownian motion of a fluorescent species in a femto liter-sized volume, yielding molecular parameters such as diffusion time and the number of particles, that can be used to assess interactions the fluorescent species with or their encapsulation within supramolecular assemblies.^[36] Accordingly, we coencapsulated Atto488-labeled single-stranded template DNA and measured the diffusion times of 488-template-CNCs in comparison to free 488-template ssDNA. The corresponding shift of the FCS autocorrelation curves to significantly higher diffusion times indicated that nanocompartments were loaded with labeled ssDNA template (Figure 5A). By applying a 2-component fit (fixing the diffusion time of free dye as one of the components), we obtained an average diffusion time $\tau_D = 4190 \mu\text{s}$ for ssDNA template-CNCs compared to $\tau_D = 151 \mu\text{s}$ of the free ssDNA template. In ssDNA template-CNCs, the fraction of free, labeled ssDNA template was 8%, indicating that most of the template DNA was present inside the CNCs (Figure 5A). The total concentration of the ssDNA template ($32 \mu\text{g mL}^{-1}$) was obtained using UV-vis spectroscopy (Table S2, Supporting Information).

By dividing the ssDNA template concentration by the number of polymersomes obtained from NTA, we determined that 2.5 ± 1 template ssDNA molecules were encapsulated per CNC on average. A standard BCA assay revealed the amount of enzyme inside the nanocompartments at $30 \mu\text{g mL}^{-1}$ for Klenow polymerase and $18.6 \mu\text{g mL}^{-1}$ for ATP sulfurylase (Figure S5, Supporting Information). Thus, the encapsulation efficiency for the Klenow fragment was $36 \pm 12\%$, and $22 \pm 4\%$ for ATP sulfurylase, which is in line with encapsulation efficiencies found for polymersomes harboring other enzymes.^[21,22] In order to exclude differences related to the number of melittin pores, both types of CNCs were permeabilized with $25 \mu\text{M}$ melittin (final concentration), which results in ≈ 100 pores per CNC.^[32,33,28]

Furthermore, we surface-functionalized CNCs with 22-mer oligonucleotides in order to ultimately anchor them to a glass surface. For this purpose, CNCs were incubated with the 22-mer bearing a cholesterol moiety at the 3' end, which inserts into the hydrophobic region of the CNC membrane (Tables S3 and S4, Supporting Information). The degree of functionalization was measured by FCS using CNCs that had been incubated with fluorescently labeled ssDNA-cholesterol (Atto488-ssDNA-cholesterol) (Table S4, Supporting Information). Based on these measurements we estimated the number of ssDNA-cholesterol strands exposed on the Klenow-CNC surface and ATP sulfurylase-CNC surface to be, respectively 18 ± 3 and 21 ± 2 . The fraction of Atto488-ssDNA-CNCs was 93%, while that of the free Atto488-ssDNA-cholesterol was 7%, indicating that most of the ssDNA-cholesterol had partitioned into the polymersome membrane (Table S4, Supporting Information).

2.2. DNA Duplex Formation in CNCs

Having determined the amount of encapsulated enzyme, we used the same enzyme concentrations in bulk experiments to evaluate the efficiency of the cascade reaction in CNCs. First, we evaluated DNA duplex formation, i.e., enzymatic activity of the Klenow fragment in Klenow-polymerase CNCs alone (Figure 4 and Table S5, Supporting Information).

DNA polymerases catalyze DNA polymerization in replication and repair, and are thus crucial for survival in all living cells. Klenow polymerase is used for annealing and primer extension, with the simultaneous release of PP_i upon addition of each nucleotide. To quantitatively assess the enzymatic activity of Klenow polymerase, we monitored DNA duplex formation by SYBR Green I (SG) fluorescence, which dramatically increases in brightness (>1000 -fold) upon interaction with double stranded DNA.^[37]

DNA polymerization, indicated by a steady increase of SG fluorescence over 1 h, took place with free enzyme and enzyme encapsulated in nanocompartments whose membrane was made porous by the insertion of melittin (Figure 5B). Conversely, Klenow polymerase did not produce any double-stranded DNA and thus, SYBR green fluorescence did not increase in CNCs that were not permeabilized (Ctrl Klenow CNC; Figure 5B, red line), as neither primers, dNTPs, nor SYBR green were able to enter the compartment. Furthermore, when nanocompartments lacked Klenow fragment

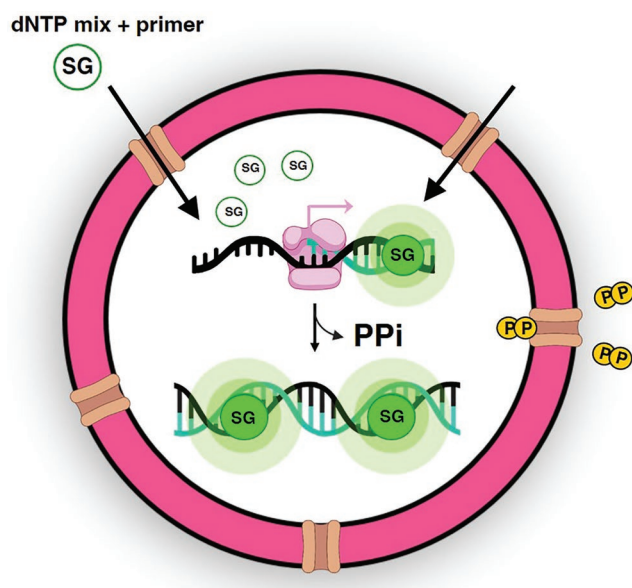


Figure 4. Detection of DNA synthesis inside Klenow-CNCs by SYBR green I. The Klenow fragment of DNA polymerase I (pink) in the core of the nanocompartment catalyzes the templated polymerization of the complementary DNA strand, accompanied by the release of PP_i which diffuses out through melittin pores. The formation of double-stranded DNA is visualized by SYBR green I (SG) which generates a fluorescent signal upon intercalation in double-stranded DNA.

or template DNA, or if dNTPs were not added to the system, double-stranded DNA was not formed and SG emitted only weak fluorescence reflecting the annealed primer (Figure S6, Supporting Information). We performed the enzyme activity measurements at 25°C because Klenow polymerase was shown to exhibit the tightest binding to primed-template DNA at this temperature.^[38,39] To examine the effect of confinement on thermal stability of the Klenow polymerase, we compared enzyme activity of Klenow CNCs to that of free enzyme at 55 and 75°C (Figure 5C,D; and Figure S7, Supporting Information). In order not to damage the photophysical properties of SG, free Klenow fragment and melittin-permeabilized Klenow CNCs were heated for 1 h at 55 and 75°C , and subsequently the reaction was monitored in the presence of SG over a period of 2 h at room temperature. Notably, when the enzyme was residing in the cavity of CNCs, DNA polymerization remained high over 2 h with a slight decrease at 75°C , whereas denaturation caused the activity of free enzyme to constantly drop at both temperatures. This apparent shielding against adverse temperature effects might be the result of molecular crowding. Consistent with this notion, it has recently been shown that the presence of trehalose in CNCs containing laccase preserved 75% of the enzyme's activity when heated at 50°C for 3 weeks.^[40] The trehalose in the cavity of the vesicles helped to maintain the structural integrity of the enzyme, probably by noncovalent interactions enabled through molecular crowding. Furthermore, enzymatic NAD^+ -regeneration silica nanoreactors showed increased resistance against heat which was attributed molecular interactions preventing structural denaturation.^[41] In Klenow CNCs, the confined template DNA and newly synthesized DNA strands might have a similar protective effect.

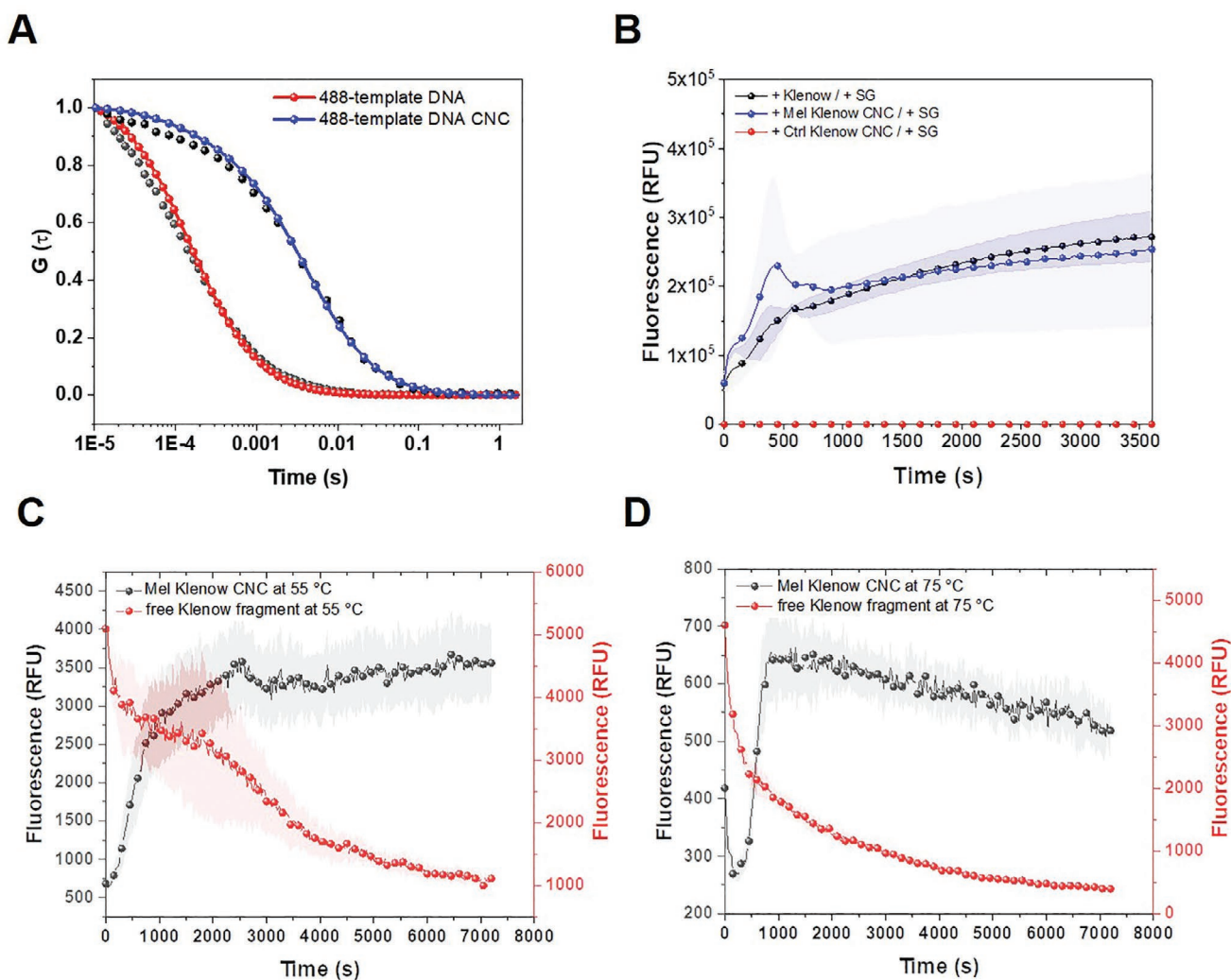


Figure 5. A) FCS autocorrelation curves of free Atto-488-template DNA (red) and Atto-488-template DNA CNC (blue). Dots: raw data. Solid line: fitted model. B) Activity of free Klenow polymerase (black), Klenow polymerase CNC with melittin (blue), Klenow polymerase CNC without melittin (red) at 25 °C. Error bands represent \pm SD, $n = 3$ replicates. C) Enzyme activity of melittin-permeabilized Klenow CNCs (red) and free Klenow fragment (black) treated for 1 h at 55 °C and D) treated for 1 h at 75 °C. Fluorescence (SG) measurements were carried out at RT. Error bands represent \pm SD, $n = 3$ replicates.

2.3. CNC Mediated Signaling Cascade in Solution

Next, we explored the signal transduction between tandem CNCs through melittin pores whereby the PPI produced by the primer-templated DNA polymerization inside Klenow-CNCs provides the “signal” for the CNC containing ATP sulfurylase (Figure 2). More specifically, we studied the two types of CNCs in close proximity on the individual reaction steps and on the overall cascade efficiency. The PPI produced by Klenow CNCs was determined by a pyrophosphate assay kit which uses a fluorogenic pyrophosphate sensor that has its fluorescence intensity at $\lambda_{\text{ex}} = 316 \text{ nm} / \lambda_{\text{em}} = 456 \text{ nm}$ proportionally dependent upon the concentration of pyrophosphate. The PPI released was found to be $3.3 < \text{PPI} > 4.3 \mu\text{M}$ after 20 min of incubation at 25 °C and $3.2 < \text{PPI} > 4.3 \mu\text{M}$ after 12 h incubation, suggesting that the reaction was completed at 20 min (Figure S8, Supporting Information). After establishing PPI

production by Klenow CNCs, the next step was to examine if the PPI was able to enter the downstream ATP sulfurylase-CNC in the cascade, where the ATP sulfurylase catalyzes its transfer to adenosine 5'-phosphosulfate (APS), yielding ATP.^[42] First, we quantified the efficiency of ATP production by ATP sulfurylase in solution using bioluminescence, which results from an ATP dependent, luciferase-catalyzed oxidation of luciferin, and generated a corresponding dose response curve (Figure S9, Supporting Information). To measure bioluminescence as final readout of the cascade reaction, we supplied luciferase and its substrate D-luciferin in solution in addition to feeding the cascade reaction with a mixture containing primer and nucleotides (dNTPs) required for DNA-templated dsDNA synthesis and APS as substrate for ATP sulfurylase (see Figure 2 above). We used luciferase from the North American firefly *Photinus pyralis*^[43] (Ppy luciferase) as a reporter enzyme for the signal transduction in CNCs because it is ATP dependent and with

0.88 photons produced per luciferin molecule consumed, it is rather efficient.^[44,45] In the presence of permeabilized CNCs, the signaling events involving the reaction products of each CNC take place upon addition of the substrate mix, ending in a steep rise of bioluminescence that peaks after a few seconds and remains constantly high for a minute or longer (Figure S10, Supporting Information). Based on the ATP-bioluminescence dose response curve, the ATP produced by the tandem CNCs, was found to be 0.9 nM at room temperature.

2.4. Spatial Integration of CNCs on ssDNA-Micropatterned Glass Surfaces

In order to produce a reusable platform of spatially organized polymersomes, we used microcontact printing on a glass surface to afford anchoring of polymersomes that were functionalized with a 22-mer oligonucleotide via hybridization of complementary DNA (Figure 6). First, the glass surface was treated with [3-(2,3-epoxypropoxy)-propyl]-trimethoxysilane. Then, amino-functionalized ssDNA (NH₂-DNA) ink was used

to print a pattern of circles, 10 μm in diameter and 10 μm apart from each other (Figure 6A). The NH₂-terminated oligonucleotide sequence includes a 5' oligothymine of nine nucleotides, followed by a random sequence of 22 nucleotides to favor duplex formation with complementary DNA at room temperature (Figure 6A(i); and Table S6, Supporting Information). The regular array of NH₂-DNA dots on the glass surface was confirmed by atomic force microscopy (AFM; Figure 6B) and by confocal laser scanning microscopy (CLSM) using fluorescently labeled NH₂-DNA (Figure 6C). AFM images of an individual dot (Figures S11 and S12, Supporting Information) revealed a height of ≈10 nm for the printed dot.

Rather than directly attaching CNCs exposing complementary DNA on their surface to the microprinted dots, we introduced an 44-mer adaptor to facilitate the molecular flow between CNCs (Figure 6A(ii); and Table S6, Supporting Information). The adaptor is partially complementary to the printed NH₂-DNA and at the same time, provides a new orthogonal DNA binding sequence with the corresponding directionality that allows for the formation of an antiparallel DNA duplex with nucleotides exposed on the surface of ssDNA-functionalized CNCs.

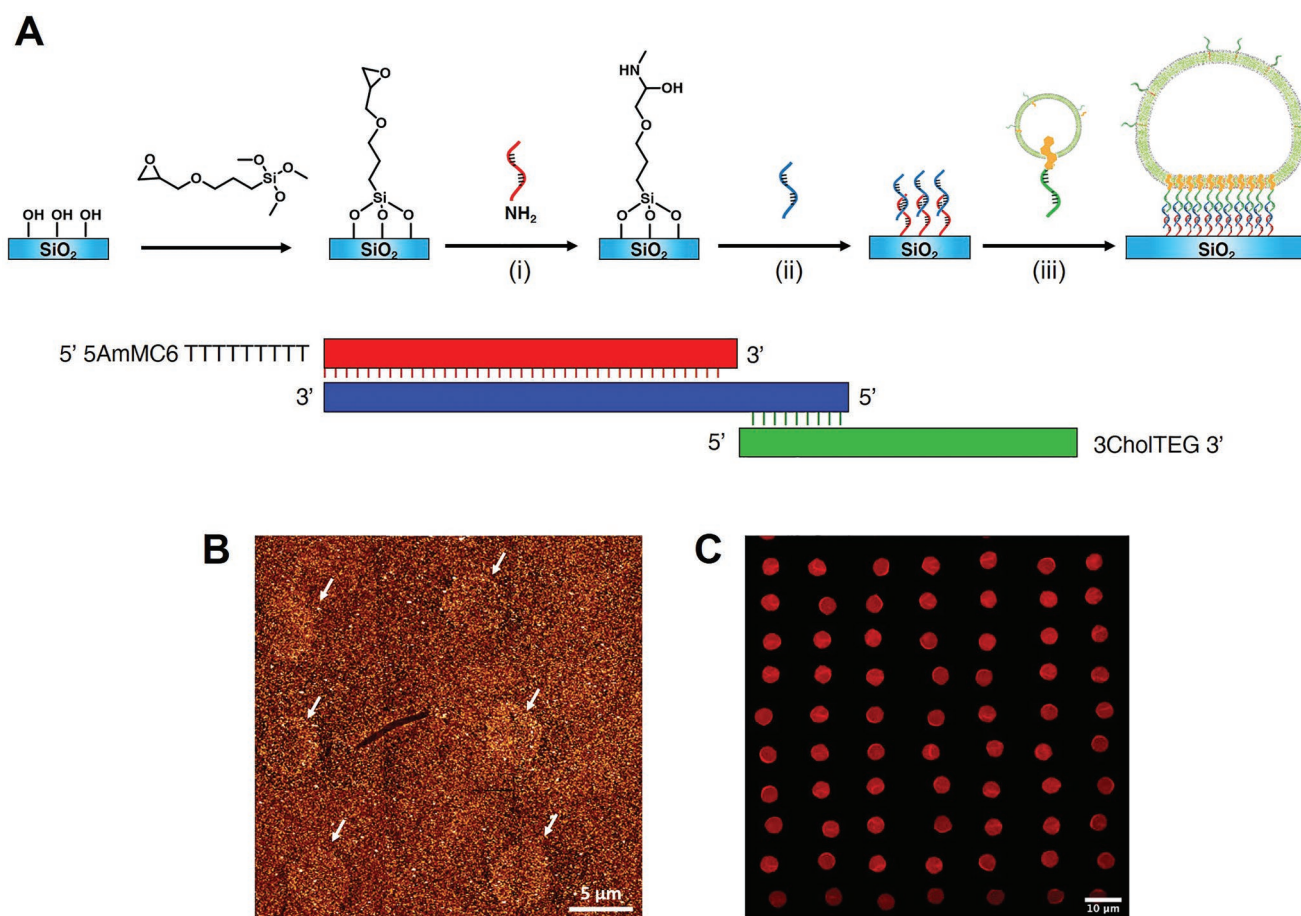


Figure 6. A) Chemical functionalization of the micro-printed glass surface with the amino-functionalized ssDNA. CNC micropatterning involving hybridization of complementary oligonucleotides. Red, NH₂-modified 31-mer microprinted on glass; blue, adaptor 44-mer; green, cholesterol anchored 22-mer exposed on the surface of CNCs (green). B) AFM height image of the DNA-functionalized glass slide recorded in 10 mM Tris-HCl buffer at pH 7.2 at the resolution of 128 lines. The overview image is compiled of 9 individual tiles (corresponding phase type overview in Figure S12, Supporting Information). The dots patterned with NH₂-DNA are marked with arrows. C) CLSM image of glass surface microprinted with Cy5-labeled NH₂-modified 31-mer.

After rinsing excess adaptor from the surface, DNA-functionalized CNCs were attached by hybridization at room temperature for 10 min (Figure 6A,(iii); and Table S6, Supporting Information).

2.5. Biomolecular Signal Transduction on a Platform of Immobilized CNCs

To establish a platform of communicating CNCs, we anchored Klenow CNCs and ATP sulfurylase CNCs at equal concentrations to the microprinted surface which we then analyzed by AFM in aqueous solution (Figure 7A,B). The surface topography of a microprinted dot indicates the presence of several attached polymersomes to it (Figure 7A). When the concentration of the polymersomes in the solution used for incubation on the surface was sufficiently low, it was possible to record a height image of a single polymersome attached to a dot (Figure 7B).

Considering that the height image of an individual, attached polymersome reveals a total height of around 120 nm, the small height variation (20 nm) along the dashed line of a dot with several polymersomes attached suggests that the entire area of the dot was covered by polymersomes, with virtually no free space between them. In the corresponding phase image, a phase shift of 1 deg was observed, indicating a rather uniform packing of polymersomes throughout the dot. The diameter of an individual polymersome measured by AFM was 250–350 nm, which taking into account a broadening by the lateral tip effect or a possible deformation upon attachment, is consistent with the size range measured by DLS (Table S3, Supporting Information).^[44] To distinguish between the two different types of CNCs on the micropatterned surface, we attached polymersomes encapsulating Atto488 or DyLight633, and examined the platform by CLSM (Figure 7C). Merging the green-channel image with the red-channel image revealed that both types of polymersomes are present on each dot. By quantifying fluorescence signals, we estimated the total number of polymersomes per DNA-printed dot to be 54 ± 9 , with a roughly equal distribution of green (29 ± 7) and red (25 ± 6) polymersomes. However, this number might be an underestimation as individual polymersomes are below the resolution limit.

The molecular signal transduction on the platform was examined by measuring bioluminescence as final readout (Figure 7D). For this purpose, complete reaction mix (CRM), i.e., the reaction mix used for initiating (dNTP, primer) and supporting (APS) the cascade, supplemented with luciferase and D-luciferin, were added to the Klenow-CNCs and ATP sulfurylase-CNCs hybridized to the microprinted dots. When both CNCs were permeabilized, a sharp rise in bioluminescence occurred with 30 s after adding CRM, indicating the production of signals required for carrying out the cascade reaction. Comparison of the peak intensity to a calibration curve for ATP-dependent bioluminescence in solution (Figure S9, Supporting Information), suggested that the signaling led to 1.1 nM ATP production by the ATP-sulfurylase-CNCs on the platform. In the absence of melittin pores, signals were not produced nor transmitted and no burst of light was detected although bioluminescence was slightly increased compared to the addition of

CRM alone. It is possible that this increase is due to residual enzyme on the outer surface of CNCs that was not removed by digestion of the CNCs with proteinase K.

2.6. Reusability of a CNC Platform

DNA hybridization as an immobilization strategy has the advantage of being a reversible process.^[46] To test the reusability of the DNA-microprinted surface as a platform for CNC immobilization, we used a quartz crystal microbalance with dissipation monitoring (QCM-D) analysis to monitor multiple cycles of CNC loading and removal by alkaline treatment (Figure 7E). QCM-D monitors changes in frequency (ΔF) inversely associated with mass deposition, and changes in dissipation (ΔD) which reveal the viscoelastic properties of the surface. QCM-D is commonly used in the analysis of vesicle adsorption on various substrates.^[47–49] Reusability of our platform afforded by reversible hybridization of complementary DNA can be demonstrated using a silica-sputtered QCM sensor functionalized with NH_2 -DNA, which was further stabilized by the addition of a blocking agent. We developed a cyclic procedure that allows for reusing the DNA-microprinted surface (Figure 7E). In the first stage, the DNA adaptor is injected to the cell with a functionalized QCM sensor in contact with Tris buffer, which results in a small change in the normalized frequency shift, signaling the attachment of the adaptor to the surface. Next, a solution containing polymersomes is injected, causing a significant drop in the frequency value due to their attachment to the surface via DNA hybridization. The associated change in the dissipation value implies that a soft material was deposited on the functionalized SiO_2 surface. After the injection of the NaOH solution, followed by a rinsing step, the polymersomes had detached, and the frequency shift increased slightly above 0 Hz, indicating that a small amount of the surface functionalization was removed along with the polymersomes. After this first conditioning step, the on-off process of polymersome attachment and detachment was repeated twice (Figure 7E). In the on-off repeats, the frequency shift reaches the same value, meaning the same mass was deposited on the surface, with the curve exhibiting an exponential shape for both the frequency and the dissipation curve. This characteristic shape has previously been reported for stable vesicle adsorption.^[50–52] The QCM-D data provide evidence that our platform can be loaded with fresh nanocompartments for repeated measurements within few hours as a stepping stone towards application.

3. Conclusion

While molecular diffusion is employed by biological systems to initiate and propagate microenvironments in the context of cell signaling, at the nanoscale it is a prime communication paradigm, which is employed to form nanonetworks. In this work, we devised and validated a reusable platform comprising an array of soft catalytic nanocompartments that can be reversibly immobilized in a distinct micropattern. The geometrical constraints conferred upon the confined reactions result in a domino effect that produces and transmits soluble messengers

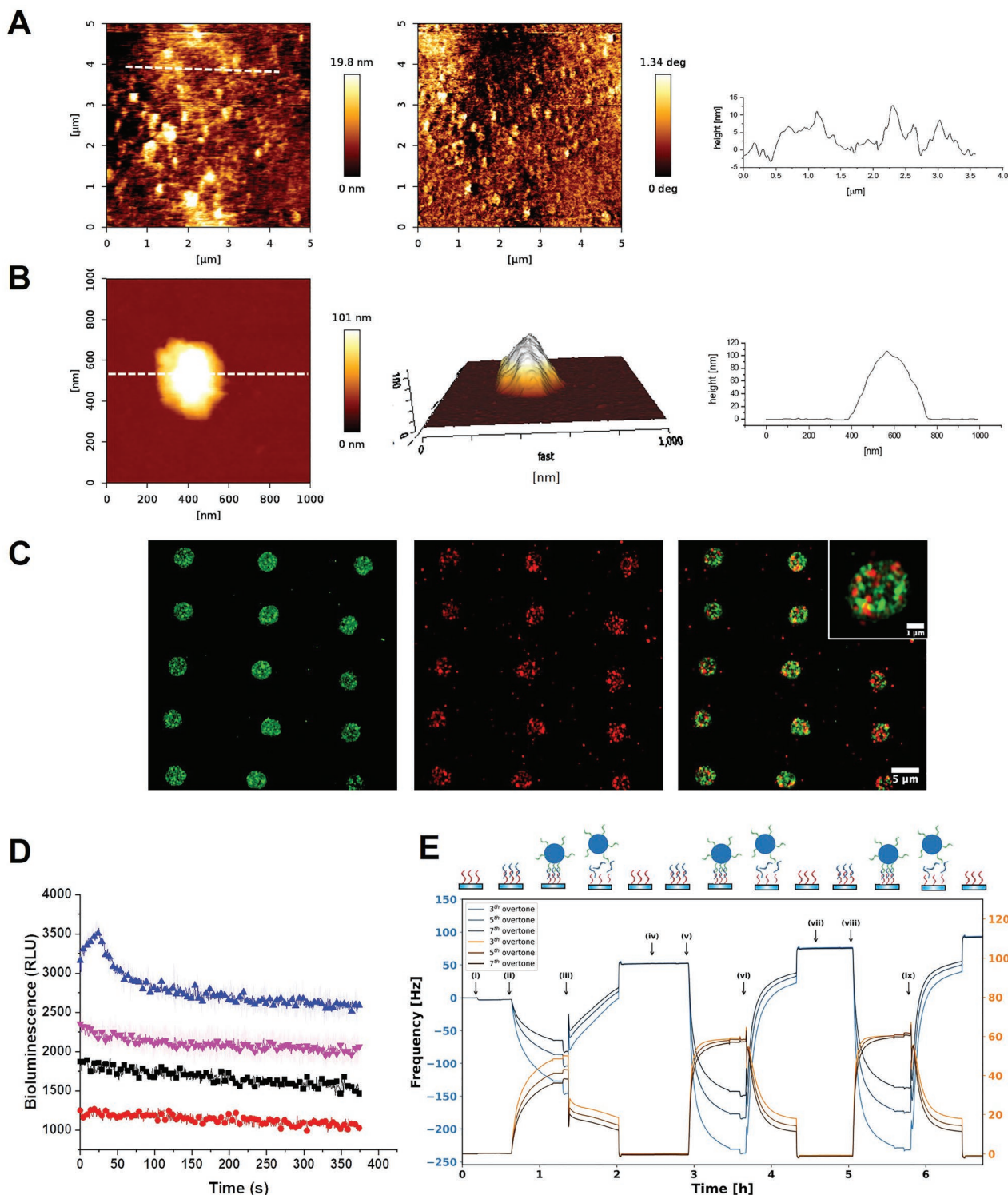


Figure 7. A) left, AFM height image, middle, phase type image, and right, height profile (corresponding to dashed white line) of tandem CNCs attached via DNA hybridization on the microprinted glass surface recorded in 10 mM Tris-HCl buffer at pH 7.2. B) left, AFM height image, middle, phase type image and right, corresponding height profile of a single CNC. C) CLSM micrographs of polymersomes labeled with either cholesterol functionalized Atto-488 (green) or Dylight-633 (red)-DNA and immobilized by hybridization on a microprinted glass surface. Left panel, 488-channel, middle panel, 633-channel, right panel, merged image. Scale bars: 5 μm . D) Bioluminescence generation by permeable Klenow-CNCs and permeable ATP sulfurylase-CNCs (blue), by nonpermeable Klenow-CNCs and nonpermeable ATP sulfurylase-CNCs (pink), by the substrate mix alone (black), and by D-Luciferin and luciferase (red). Error bands represent $\pm\text{SD}$, $n = 3$ replicates. E) QCM-D measurement of immobilized CNCs following repeated loading-removal cycles. Frequency (blue) and dissipation (brown) were recorded at three overtones ($n = 3, 5, 7$) as a function of time. (i, iv, vii) Addition of adaptor DNA, (ii, v, viii) immobilization of 22-mer polymersomes, and (iii, vi, ix) separation of DNA strands with 1 M NaOH.

such as PPI and ATP. Corresponding polymer-based nanocompartment assemblies offer an ideal scaffold for the development of the next generation responsive and communicative soft-matter analytical devices which might allow for the detection of dysregulated signal transduction pathways associated with different diseases.

4. Experimental Section

Materials: Micro contact printed surfaces were purchased from n.able GmbH (Germany). The dNTP Mix was purchased from Thermo Fisher Scientific (USA). The DNA polymerase I, Large (Klenow) Fragment was purchased from New England Biolabs (UK). ATP sulfurylase from *S. cerevisiae*, Recombinant was purchased from Creative Enzymes (USA). Luciferase from *Photinus pyralis* (firefly), D-Luciferin, and adenosine 5'-phosphosulfate sodium salt were purchased from Sigma-Aldrich (USA), as well as the pyrophosphate assay kit and the ATP colorimetric/fluorometric assay kit. The DNA template, DNA primer, DNA cholesterol, DNA adaptor, and amino DNA bounded to the surface were purchased from Microsynth, Switzerland. All solvents were purchased from Sigma-Aldrich unless stated otherwise.

Functional Amphiphilic Block Copolymers: Synthesis and Characterization: PDMS_{25-b}-PMOXA₁₀ diblock copolymers were synthesized according to a previously published procedure.^[31] The molecular weights, block ratio, and chemical structures were characterized by ¹H NMR spectroscopy. The averaged molecular weight and polydispersity index (PDI) were characterized by gel permeation chromatography (GPC, Polymer Standard Services, Germany) with PS beads as the solid phase and CHCl₃ as the running phase (1.0 mL min⁻¹ flow rate). The GPC traces were recorded using a refractive index detector.

DNA Polymerase CNC: CNCs were prepared at RT, with 50% (molar ratio) of the azide-functionalized polymer. Films were rehydrated to a final polymer concentration of 5 mg mL⁻¹ with 10 μL of DNA Polymerase I, Large (Klenow) Fragment (5000 U mL⁻¹), 10 μL of DNA template (20 nmol), and 25 μL of melittin 1 mM (from bee venom) in 10 mM Tris-HCl, 5 mM MgCl₂ (pH 7). The solution was stirred at 300 rpm for 12 h at r.t. Samples were extruded 11 times through an Avanti mini-extruder (Avanti Polar Lipids, USA) with a 200 nm pore diameter polycarbonate membrane. Nonencapsulated enzyme was removed through size exclusion chromatography (SEC) (Sephacrose 4B column; 30 cm length) and recovered for quantification. For control experiments, polymersomes with encapsulated enzymes but without melittin were prepared using the same method as above.

ATP Sulfurylase CNC: CNCs were prepared at RT, with 50% (molar ratio) of the azide-functionalized polymer. Films were rehydrated to a final polymer concentration of 5 mg mL⁻¹ with 10 μL of ATP Sulfurylase from *S. cerevisiae* (2 U mL⁻¹) in 10 mM Tris-HCl, 5 mM MgCl₂ (pH 7), and 25 μL of melittin 1 mM (from bee venom). The solution was stirred at 300 rpm for 12 h at r.t. Samples were extruded 11 times through an Avanti mini-extruder (Avanti Polar Lipids, USA) with a 200 nm pore diameter polycarbonate membrane. Nonencapsulated enzyme was removed through SEC (Sephacrose 4B column; 30 cm length) and recovered for quantification. For control experiments, polymersomes with encapsulated enzymes but without melittin were prepared using the same method as above.

CNC Characterization—Fluorescence correlation spectroscopy (FCS): To quantify the number of DNA template in the inner core of the nanocompartments, a labeled DNA template (5'-Atto488-TCT AGA TTA CCG CGA TCT AGC CTT ATG GCC TAG TAA GTG TCC GAA CGA TGG CTA GTA GTC GAT TAA TTG G-3') was encapsulated in CNC. All measurements were carried out using an LSM 880 confocal laser scanning microscope (Carl Zeiss, Germany) with a 40 × 1.2 water immersion C-Apochromat objective lens. Measurements were performed at RT using a sample volume of 20 μL on a 22 × 50 mm glass slide. A He-Ne laser at 488 nm was used for excitation of the Atto488 template, at 1% attenuation and pinhole 43 μm. The fluorescence signal was

measured in real time, and the autocorrelation function was calculated by the software calculator QuickFit 3.0.29. Measurements were recorded over 5 s, and each measurement was repeated 30 times. Autocorrelation curves were fitted by a two-component model (Equation (1)), except for dye-only samples

$$G(\tau) = 1 + \left(1 + \frac{T}{1-T} e^{-\frac{\tau}{\tau_{\text{trip}}}} \right) \frac{1}{N} \left(\frac{f_1}{1 + \frac{\tau}{\tau_{D1}} \sqrt{1 + R^2 \frac{\tau}{\tau_{D1}}}} + \frac{f_2}{1 + \frac{\tau}{\tau_{D2}} \sqrt{1 + R^2 \frac{\tau}{\tau_{D2}}}} \right) \quad (1)$$

Where f_1 and f_2 are, respectively, the fraction of the particles of the corresponding component 1 (dye) or 2 (vesicles), τ_{D1} represents the diffusion time of the dye and τ_{D2} the diffusion time of the vesicles, T is the fraction of fluorophores in triplet state with triplet time τ_{trip} , N is the number of particles, and R is the structural parameter, fixed at 5, according to the manufacturer's guidelines. The τ_{trip} and τ_D of free dye were determined independently, and subsequently fixed in the fitting procedure for dye-stained vesicles.

The degree of labeling (DOL) was obtained from the ratio of the counts per molecule (CPM)

$$\text{DOL} = \frac{\text{CPM}_{\text{labeled DNA template}}}{\text{CPM}_{\text{free dye}}} \quad (2)$$

Similarly, the DNA template per vesicle were obtained by

$$N_{\text{DNA template}} = \frac{\text{CPM}_{\text{vesicle}}}{\text{CPM}_{\text{labeled DNA template}}} \quad (3)$$

To quantify the DNA strands exposed on CNCs, Cholesterol DNA labeled with Atto488 was used. An excess amount (10 μL of a 200 μM stock) was added to vesicles and purified via SEC.

$$N_{\text{strands}} = \frac{\text{CPM}_{\text{vesicle}}}{\text{CPM}_{\text{labeled DNA}}} \quad (4)$$

Static (SLS) and Dynamic (DLS) Light Scattering: SLS and DLS experiments were performed on a setup from LS instruments (Switzerland), equipped with a He-Ne 21 mW laser ($\lambda = 632.8$ nm) at scattering angles from 30° to 55° at 25 °C. The radius of gyration (R_g) was obtained from the SLS data with a Guinier plot. The intensity versus angle curve of a diluted sample (to suppress multiple scattering) was fit with a linear regression and the slope of the curve m was used to calculate R_g according to the equation

$$R_g = 10^9 \times \sqrt{3m} \quad (5)$$

The error was calculated on the standard error of the slope. In the case of SLS, second order cumulant analysis of the data between 30° and 155° was performed to obtain the R_h .

TEM: CNC suspensions in PBS at 0.25 mg mL⁻¹ were deposited on glow-discharged carbon grids (Quantifoil, Germany) stained with 1.5% uranyl acetate solution and deposited on carbon-coated copper grids. Micrographs of nanostructures were recorded on a Philips CM100 transmission electron microscope at an accelerating voltage of 80 kV.

NTA: NTA was used as further analysis of particle size and concentration, on a NanoSight NS300 (Malvern Panalytical Ltd., UK), using a flow cell (100 μL min⁻¹), 1:1000 concentration in freshly filtered PBS, yielding particle R_h and concentration (particle mL⁻¹).

Enzyme Quantification: The encapsulation efficiency of DNA polymerase and ATP sulfurylase in CNCs was calculated using the enhanced Pierce Bicinchoninic Acid (BCA) assay according to the supplier's protocol. CNCs were ruptured first by sonication and then incubated with ethanol in a ratio of 3:1, at 37 °C for 1 h. The solution was filtered through 0.2 μm nylon membrane, 4 mm filter (Whatman, General Electric, UK) and used in a 1:2 ratio to the working reagent for the assay. The mixtures of standards and samples were incubated for 2 h at 37 °C and the absorbance was measured at 562 nm using a SpectraMax plate reader.

UV-Vis Spectroscopy: A 3.0 μL sample of enzyme was analyzed at OD280 using a Nanodrop ND-1000 spectrophotometer and blanked

with 10 mM Tris-HCl, 5 mM MgCl₂. The observed average measurement of 3 replicate samples at 280 nm was converted to mg mL⁻¹ using an extinction coefficient of 55450 M⁻¹ cm⁻¹ and a molecular weight of 68067 Daltons for Klenow polymerase, and an extinction coefficient of 61310 M⁻¹ cm⁻¹ and a molecular weight of 57753 Daltons for ATP sulfurylase.

Klenow CNC—Enzymatic Assay: Fluorescence spectra of Klenow CNCs (with or without melittin), free SG and SG in complex with DNA were measured on a Spectramax id3 plate reader at room temperature. 200 μL of the reaction mix consisting of 10 μL of CNC, 1 μL of dNTP Mix (10 mM), 1 μL of primer (200 nM), and 1 μL (1X concentration) of LightCycler-FastStart DNA Master SYBR Green (Roche Diagnostics GmbH) in 10 mM Tris-HCl, 5 mM MgCl₂ was added in each well of a 96 well plate. SG was excited at 485 nm and the fluorescence monitored over 1 h.

Pi Quantification: The pyrophosphate produced by DNA polymerase CNC was calculated using the pyrophosphate assay kit according to the supplier's protocol. The pyrophosphate concentration of CNCs was determined by a fluorogenic pyrophosphate sensor monitoring the fluorescence intensity ($\lambda_{\text{ex}} = 316 \text{ nm}/\lambda_{\text{em}} = 456 \text{ nm}$). 50 μL of the Master Reaction Mix was added to 50 μL of the sample, blank and standard, the wells were mixed using a horizontal shaker and the reaction incubated for 30 min at room temperature in the dark.

Klenow Polymerase-ATP Sulfurylase CNC Cascade in Solution: Luminescence spectra of CNCs (with or without melittin) were measured on a Spectramax id3 plate reader at room temperature by scanning from 400 to 800 nm. One-pot reaction mixture was prepared including 10 μL of DNA polymerase CNC, 10 μL of ATP sulfurylase CNC, 1 μL of dNTP Mix (10 mM), 1 μL of primer (200 nM), 2 μL of APS (11 mM), 1 μL of Luciferase (2 mg mL⁻¹) and 2 μL of D-Luciferin (10 mM) in 10 mM Tris-HCl, 5 mM MgCl₂. 200 μL of the reaction mix was added in each well of a 96 well plate and the luminescence monitored over a period of 1 h.

ATP Quantification: The ATP produced by the DNA polymerase CNC and the ATP sulfurylase CNC acting in tandem was calculated using the ATP Colorimetric/Fluorometric Assay kit according to the supplier's protocol. 50 μL of the Fluorometric Reaction Mix was added to 50 μL of the sample, blank, and standard. The wells were incubated at room temperature in the dark for 30 min and the fluorescence intensity monitored on a Spectramax id3 plate reader ($\lambda_{\text{ex}} = 535 \text{ nm}/\lambda_{\text{em}} = 587 \text{ nm}$). The fluorometric product is proportional to the amount of ATP present.

DNA Ink: DNA-NH₂ was dissolved in milli-Q water to a 100 μM stock solution. To prepare the ink for printing 1 μL of the stock DNA, 2 μL of water and 1 μL of glycerol were mixed to achieve 25 μM printing DNA solution. From such prepared ink 0.5 μL was used to load onto the plasma activated (2 min O₂ plasma, Diener Atto) SPT probe (SPT-30S, BioForce Nanosciences, Inc., USA).

3-Glycidoxypropyltrimethoxysilane (GPTMS) Substrates: Substrates were functionalized by immersing cleaned (5 min sonication in chloroform, ethanol and water in each step, and plasma activated (2 min O₂ plasma, Diener Atto) glass slides in a solution of 1% GPTMS in toluene for 2 h at RT under inert gas. Next, glass slides were washed with acetone and ethanol and blow dried with N₂. Functionalized substrates were stored in a desiccator until used.

Printing DNA Arrays: Printing the samples was executed on Molecular Printer (n.able GmbH, Germany). Ink loaded SPT probe was loaded onto the printer and a patterning assistant was used to define the number of spots in X and Y direction covering total of 2500 × 2500 μm. Printing was executed automatically by the instrument under ambient temperature and relative humidity of 50%. After printing samples are packed in a vacuum bag and stored until used.

Polymersome Functionalization with DNA Cholesterol: Polymersomes were functionalized with cholesterol-DNA and subsequently immobilized on the ssDNA micropatterned glass surface (2500 × 2500 μm). 100 nm cholesterol DNA was added to a solution of concentrated polymersomes and left for membrane insertion for 15–30 min.

Coimmobilization of Polymersomes on Surface: The patterned surface was covered with 100 nm adaptor DNA solution for five minutes. After washing the surface several times with PBS or 10 mM Tris-HCl, 5 mM MgCl₂, polymersomes were added onto the surface for hybridization

(15 min) and the surface was washed again several times with PBS. A Zeiss LSM880 with an attached airyscan detector was used to take images of the patterned surfaces with a water immersion objective (C-Apochromat 40x/1.2 W Korr FCS M27) and an inserted main beam splitter (488/561/633). An Ar-Laser (488 nm, 2%) and a HeNe-Laser (633, 0.5%) were used to excite the dyes and emission was filtered (BP 495–550 + LP 570) before the airyscan detector in SR mode. The recorded airyscan images (pixel diameter 50 nm) were processed in the ZEN software. Subsequently, polymersomes were counted per dot with a self-written macro in Fiji.

Klenow Polymerase-ATP Sulfurylase CNC Cascade on Surface: Luminescence on the ssDNA micropatterned surface were measured in a 24 well plate on a Spectramax id3 plate reader at room temperature by scanning from 400 to 800 nm. One-pot reaction mixture was prepared including 10 μL of DNA polymerase CNC, 10 μL of ATP sulfurylase CNC, 1 μL of dNTP Mix (10 mM), 1 μL of primer (200 nM), 2 μL of APS (11 mM), 1 μL of Luciferase (2 mg mL⁻¹), and 2 μL of D-Luciferin (10 mM) in 10 mM Tris-HCl, 5 mM MgCl₂. 200 μL of the reaction mix was added in each well of a 96 well plate and the luminescence monitored over a period of 1 h.

AFM on Surface: The AFM imaging of the DNA-functionalized glass slide was carried out using a JPK NanoWizard 3 AFM (JPK Instruments AG). The measurements were performed in the AC mode. Silicon cantilevers Multi75G and Multi 75GD-G (Budget Sensors) were used for measurements in air and PBS buffer, respectively, both with a nominal spring constant of 3 N m⁻¹ and a resonance frequency of 75 kHz. The images were collected with a solution of 1024×1024 pixels at a scanning rate 0.3 Hz. First, the DNA-functionalized glass slides were fixed on the bottom of the a round well of 2 cm in diameter and then 2 mL PBS were added to rehydrate the surface prior to the AFM measurement. Then, the solution of the DNA adaptor at 1 μM concentration was added to the well and it was left in contact with the glass slide for 5 min. Following, the solution containing the adaptor was removed, the well was rinsed with another portion of the PBS buffer and finally rehydrated prior to the measurement. The images were analyzed using JPK data processing software.

Quartz Crystal Microbalance with Dissipation Monitoring (QCM-D) on Surface: SiO₂ sputtered QCM-D sensors (5 MHz, Biolin Scientific) were modified with a 1% (w/w, 1:1) mixture of (3-glycidyloxypropyl) trimethoxysilan and ethyl-trimethoxysilane similar to a procedure reported by Rigo et al.^[53], followed by functionalization with NH₂-DNA in 0.1 M KOH (pH 8.5) at 37 °C for 2 h. QCM-D was performed with a Q-Sense E1 system (Biolin Scientific, Sweden). Measurements were recorded at multiple overtones. The sensor was equilibrated with 10 mM Tris-HCl, 5 mM MgCl₂ (washing buffer). DNA adaptor was added under continuous flow of 100 μL min⁻¹ and left to hybridize for 15 min. Nonhybridized DNA was washed away (0.6 μL min⁻¹, 1.2 mL) with washing buffer. 22-mer polymersomes were added under continuous flow of 100 μL min⁻¹ and left to hybridize for 30 min. Again, the sensor was washed with washing buffer (0.6 μL min⁻¹, 1.2 mL). MilliQ water was flowed through the system (0.6 μL min⁻¹, 1.2 mL) before 1 M NaOH was used to separate DNA strands under continuous flow (0.1 μL min⁻¹, 4 mL). MilliQ water was used (0.6 μL min⁻¹, 1.2 mL) as an intermediate step before the sensor was equilibrated again with washing buffer (0.6 μL min⁻¹, 1.2 mL). This procedure was repeated twice.

Supporting Information

Supporting Information is available from the Wiley Online Library or from the author.

Acknowledgements

The authors thank Dr. Miguel Angel Aleman Garcia for preliminary design of the surface patterning with DNA and Dr. Riccardo Wehr

for providing PMOXA₁₀-b-PDMS₂₅. They also gratefully acknowledge many fruitful discussions with Prof. Wolfgang Meier, who has sadly passed away. The authors wish to thank the Swiss National Science Foundation, the National Centre of Competence in Research – Molecular Systems Engineering (NCCR-MSE) and the University of Basel for the funding. Schematic figures were created in part with BioRender.com (2022).

Open access funding provided by Universitat Basel.

Conflict of Interest

The authors declare no conflict of interest.

Author Contributions

Conceptualization, project administration and supervision: C.E.H., C.G.P., V.M.; funding acquisition C.E.H., C.G.P.; investigation and methodology: V.M., D.H.; formal analysis: V.M., D.H., A.K.; visualization: V.M., C.S., D.H., A.K.; part contributions to manuscript: D.H., A.K.; writing – original draft: V.M., C.S.; writing – review: all authors; writing – finalization of manuscript: V.M., C.S.

Data Availability Statement

The data that support the findings of this study are available from the corresponding author upon reasonable request.

Keywords

catalytic nanocompartments, DNA hybridization, DNA micropatterning, mimics of signaling pathways, polymersomes arrays

Received: May 6, 2022

Revised: June 17, 2022

Published online: July 22, 2022

- [1] D. Qin, Y. Xia, G. M. Whitesides, *Nat. Protoc.* **2010**, *5*, 491.
- [2] B. D. Gates, Q. Xu, M. Stewart, D. Ryan, C. G. Willson, G. M. Whitesides, *Chem. Rev.* **2005**, *105*, 1171.
- [3] G. Liu, S. H. Petrosko, Z. Zheng, C. A. Mirkin, *Chem. Rev.* **2020**, *120*, 6009.
- [4] K. Salaita, Y. Wang, C. A. Mirkin, *Nat. Nanotech.* **2007**, *2*, 145.
- [5] A. K. Shukla, G. Gao, B. S. Kim, *Micromachines* **2022**, *13*, 155.
- [6] S. Im, G. Choe, J. M. Seok, S. J. Yeo, J. H. Lee, W. D. Kim, J. Y. Lee, S. A. Park, *Int. J. Biol. Macromol.* **2022**, *205*, 520.
- [7] A.-K. Amler, A. Thomas, S. Tüzüner, T. Lam, M.-A. Geiger, A.-E. Kreuder, C. Palmer, S. Nahles, R. Lauster, L. Kloke, *Sci. Rep.* **2021**, *11*, 4876.
- [8] K. Li, A. Faulkner-Jones, A. R. Dun, J. Jin, P. Chen, Y. Xing, Z. Yang, Z. Li, W. Shu, D. Liu, R. R. Duncan, *Angew. Chem., Int. Ed.* **2015**, *54*, 3957.
- [9] N. Di Marzio, D. Eglin, T. Serra, L. Moroni, *Front. Bioeng. Biotechnol.* **2020**, *8*, 326.
- [10] Y. Zhang, L. Zhu, J. Tian, L. Zhu, X. Ma, X. He, K. Huang, F. Ren, W. Xu, *Adv. Sci.* **2021**, *8*, 2100216.
- [11] I. Bernardeschi, O. Tricinci, V. Mattoli, C. Filippeschi, B. Mazzolai, L. Beccai, *ACS Appl. Mater. Interfaces* **2016**, *8*, 25019.
- [12] S. Rigo, G. Gunkel-Grabole, W. Meier, C. G. Palivan, *Langmuir* **2019**, *35*, 4557.
- [13] S. Rigo, C. Cai, G. Gunkel-Grabole, L. Maurizi, X. Zhang, J. Xu, C. G. Palivan, *Adv. Sci.* **2018**, *5*, 1700892.
- [14] B. Iyisan, A. Janke, P. Reichenbach, L. M. Eng, D. Appelhans, B. Voit, *ACS Appl. Mater. Interfaces* **2016**, *8*, 15788.
- [15] R. Booth, Y. Qiao, M. Li, S. Mann, *Angew. Chem., Int. Ed.* **2019**, *58*, 9120.
- [16] Y. Chen, M. Yuan, Y. Zhang, S. Liu, X. Yang, K. Wang, J. Liu, *Chem. Sci.* **2020**, *11*, 8617.
- [17] V. Chimisso, V. Maffei, D. Hürlimann, C. G. Palivan, W. Meier, *Macromol. Biosci.* **2020**, *20*, 1900257.
- [18] C. G. Palivan, R. Goers, A. Najer, X. Zhang, A. Car, W. Meier, *Chem. Soc. Rev.* **2016**, *45*, 377.
- [19] F. Itel, M. Chami, A. Najer, S. Lörcher, D. Wu, I. A. Dinu, W. Meier, *Macromolecules* **2014**, *47*, 7588.
- [20] J. Liu, V. Postupalenko, S. Lörcher, D. Wu, M. Chami, W. Meier, C. G. Palivan, *Nano Lett.* **2016**, *16*, 7128.
- [21] C. E. Meyer, J. Liu, I. Craciun, D. Wu, H. Wang, M. Xie, M. Fussenegger, C. G. Palivan, *Small* **2020**, *16*, 1906492.
- [22] V. Maffei, A. Belluati, I. Craciun, D. Wu, S. Novak, C.-A. Schoenenberger, C. G. Palivan, *Chem. Sci.* **2021**, *12*, 12274.
- [23] L. Zartner, V. Maffei, C.-A. Schoenenberger, I. A. Dinu, C. G. Palivan, *J. Mater. Chem. B* **2021**, *9*, 9012.
- [24] A. Wang, Y. Zheng, W. Zhu, L. Yang, Y. Yang, J. Peng, *Biomolecules* **2022**, *12*, 118.
- [25] L. Dzantiev, L. J. Romano, *Biochemistry* **2000**, *39*, 356.
- [26] T. C. Ullrich, M. Blaesse, R. Huber, *EMBO J.* **2001**, *20*, 316.
- [27] T. Pozzo, F. Akter, Y. Nomura, A. Y. Louie, Y. Yokobayashi, *ACS Omega* **2018**, *3*, 2628.
- [28] R. Wehr, E. C. dos Santos, M. S. Muthwill, V. Chimisso, J. Gaitzsch, W. Meier, *Polym. Chem.* **2021**, *12*, 5377.
- [29] A. Belluati, V. Mikhalevich, S. Yorulmaz Avsar, D. Daubian, I. Craciun, M. Chami, W. P. Meier, C. G. Palivan, *Biomacromolecules* **2020**, *21*, 701.
- [30] M. Garni, S. Thamboo, C.-A. Schoenenberger, C. G. Palivan, *Biochim. Biophys. Acta Biomembr.* **2017**, *1859*, 619.
- [31] C. E. Meyer, I. Craciun, C.-A. Schoenenberger, R. Wehr, C. G. Palivan, *Nanoscale* **2021**, *13*, 66.
- [32] M. Korpidou, V. Maffei, I. A. Dinu, C.-A. Schoenenberger, W. Meier, C. G. Palivan, *J. Mater. Chem. B* **2022**, *10*, 3916.
- [33] A. Sepehri, L. PeBenito, A. Pino-Angeles, T. Lazaridis, *Biophys. J.* **2020**, *118*, 1901.
- [34] A. E. Pittman, B. P. Marsh, G. M. King, *Langmuir* **2018**, *34*, 8393.
- [35] L. Deng, X. Huang, J. Ren, *Anal. Chem.* **2020**, *92*, 7020.
- [36] T. Einfalt, D. Witzigmann, C. Edlinger, S. Sieber, R. Goers, A. Najer, M. Spulber, O. Onaca-Fischer, J. Huwyler, C. G. Palivan, *Nat. Commun.* **2018**, *9*, 1127.
- [37] A. I. Dragan, R. Pavlovic, J. B. McGivney, J. R. Casas-Finet, E. S. Bishop, R. J. Strouse, M. A. Schenerman, C. D. Geddes, *J. Fluoresc.* **2012**, *22*, 1189.
- [38] K. Datta, A. J. Wowor, A. J. Richard, V. J. LiCata, *Biophys. J.* **2006**, *90*, 1739.
- [39] A. J. Richard, C.-C. Liu, A. L. Klinger, M. J. Todd, T. M. Mezzasalma, V. J. LiCata, *Biochim. Biophys. Acta Proteins Proteom.* **2006**, *1764*, 1546.
- [40] M. V. Dinu, I. A. Dinu, S. S. Saxer, W. Meier, U. Pielas, N. Bruns, *Biomacromolecules* **2021**, *22*, 134.
- [41] S.-M. Jo, F. R. Wurm, K. Landfester, *Angew. Chem., Int. Ed.* **2021**, *60*, 7728.
- [42] E. Bernhard, Y. Nitschke, G. Khursigara, Y. Sabbagh, Y. Wang, F. Rutsch, *J. Clin. Endocrinol. Metab.* **2022**, *107*, 109.
- [43] E. Conti, N. P. Franks, P. Brick, *Structure* **1996**, *4*, 287.
- [44] K. Jaskiewicz, M. Makowski, M. Kappl, K. Landfester, A. Kroeger, *Langmuir* **2012**, *28*, 12629.
- [45] I. N. Westensee, E. Brodzkij, X. Qian, T. F. Marcelino, K. Lefkimmatis, B. Städler, *Small* **2021**, *17*, 2007959.

- [46] J. H. Monserud, D. K. Schwartz, *ACS Nano* **2014**, *8*, 4488.
- [47] M. Kyropoulou, S. Yorulmaz Avsar, C.-A. Schoenenberger, C. G. Palivan, W. P. Meier, *Nanoscale* **2021**, *13*, 6944.
- [48] B. K. Yoon, W.-Y. Jeon, T. N. Sut, N.-J. Cho, J. A. Jackman, *ACS Nano* **2021**, *15*, 125.
- [49] N.-J. Cho, C. W. Frank, B. Kasemo, F. Höök, *Nat. Protoc.* **2010**, *5*, 1096.
- [50] E. Reimhult, F. Höök, B. Kasemo, *Langmuir* **2003**, *19*, 1681.
- [51] J. A. Jackman, G. H. Zan, V. P. Zhdanov, N.-J. Cho, *J. Phys. Chem. B* **2013**, *117*, 16117.
- [52] N.-J. Cho, S.-J. Cho, K. H. Cheong, J. S. Glenn, C. W. Frank, *J. Am. Chem. Soc.* **2007**, *129*, 10050.
- [53] S. Rigo, D. Hürliemann, L. Marot, M. Malmsten, W. Meier, C. G. Palivan, *ACS Appl. Bio Mater.* **2020**, *3*, 1533.